OPEN ACCESS

University of BRISTOL

Peer reviewed version

Link to published version (if available):
10.4271/2015-01-2568

Link to publication record in Explore Bristol Research
PDF-document

University of Bristol - Explore Bristol Research
General rights

Reduced Order Model Approach for Efficient Aircraft Loads Prediction

Author, co-author (Do NOT enter this information. It will be pulled from participant tab in MyTechZone)

Affiliation (Do NOT enter this information. It will be pulled from participant tab in MyTechZone)

Abstract

Flight loads calculations play a fundamental role in the development and certification of an aircraft and have an impact on the structural sizing and weight. The number of load cases required by the airworthiness regulations is in the order of tens of thousands and the analysis must be repeated for each design iteration. On large aircraft, CS-25 explicitly requires taking into account for loads prediction, airframe flexibility, unsteady aerodynamics and interaction of systems and structure, leading to computationally expensive numerical models. Thus there is a clear benefit in speeding-up this calculation process. This paper presents a methodology aiming to significantly reduce the computational time to predict loads due to gust and maneuvers. The procedure is based on Model Order Reduction, whose goal is the generation of a Reduced Order Model (ROM) able to limit the computational cost compared to a full analysis whilst retaining accuracy. The method is applied to a commercial transport aircraft modeled with beam elements, unsteady aerodynamics based on Doublet Lattice Method and servo-hydraulic actuators for the control surfaces. The aeroelastic equations of motion are formulated in the time-domain, through the Rational Function Approximation and application of the Balanced Truncation method. The results obtained with the reduced model shows a very good accuracy with respect to the full model and a significant saving in computational time. The impact of flexibility on the gust load factor is also highlighted, comparing it with the quasi-static analysis by Pratt's formula, current standard for Part 23 aircraft.

Introduction

Flight loads calculation is one of the first and most important processes in the design and certification of an aircraft. The certification specifications for large aircraft, EASA CS-25 and FAA FAR-25 [1,2], mandate for rational analysis taking into account all the relevant structural degrees of freedom, unsteady aerodynamics and interaction of structure and systems, which dictate the use of complex aeroelastic models [3]. Besides, the number of load cases to be considered to assure structural integrity can easily reach the order of hundreds of thousands. For all these reasons, the turnaround time of loads calculation is high and impacts on the downstream activities; therefore there is a clear benefit in speeding it up.

The common industrial approach is to generate a numerical model based on a Finite Element discretization of the airframe and unsteady aerodynamics. Whereas classical aeroelastic analyses have been performed routinely in frequency domain [4], when actuators driving control surfaces and control laws are considered it is easier to cast the equations in time domain [5] to obtain a Linear Time Invariant (LTI) state-space model. This also allows reducing the size of the model applying Model Order Reduction (MOR) techniques [6]. These techniques produce Reduced Order Models (ROM) which are capable of retaining the accuracy of the original model, but with a significant reduction of computational time.

In this paper a reduced order aeroservoelastic model of a generic transport aircraft is developed for gust and flight maneuvers responses and a MOR technique applied to reduce its size and show the advantage in terms of calculation time and loads prediction accuracy.

The paper is organized as follows: in the first section the building blocks of the aeroservoelastic model are presented, i.e. structure, aerodynamics and control surfaces actuators. A time domain state-space model is generated and its size reduced to obtain the ROM. Discrete gust responses and pitching maneuver simulations according to the certification specifications are then performed to compute airframe loads and assess the validity of the approach and the saving in computational time. A brief comparison of the gust load factor and wing loads obtained through a dynamic response analysis and through the application of a quasi-static methodology such as Pratt's formula, currently the standard for Part 23 aircraft, is also presented.

Aeroservoelastic Model

Flight loads calculations are typically performed using an aeroservoelastic model of the aircraft capable of representing, with a different degree of fidelity and uncertainty according to the phase of the development cycle, the vibration behavior over a frequency range of interest, the aerodynamics characteristics, including control surfaces, and the interaction of systems and structure (as stated in CS 25.302), mainly the Flight Control System.

The procedure proposed in this work is applied to a generic commercial transport aircraft, depicted in Figure 1; its main geometric and mass properties are summarized in Table 1. This model was developed as a part of the EU funded FFAST FP7 project. The building blocks of the aeroservoelastic model are now presented.
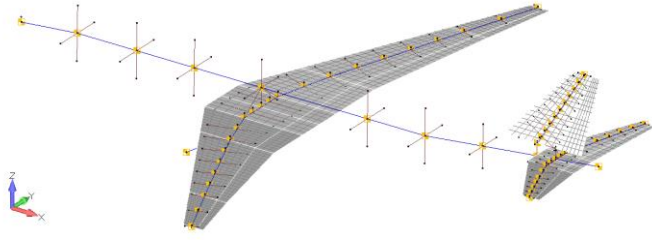
Figure 1. Aeroelastic model of the generic commercial transport aircraft

Table 1. Main properties of the generic commercial transport aircraft

Property	Value
Length	$67m$
Wingspan	$65m$
Height	$17m$
Wing area	$445m^2$
Mean Aerodynamic Chord	$6.07m$
MTOW	$268tons$
Empty weight	$192tons$
Cruise Mach	0.85
Max operating Mach	0.89
Max operating altitude	$43000ft$
M_A	0.82
M_C	0.89
M_D	0.95
$n_{z,max}$	$2.5g$
$n_{z,min}$	$-1g$

Structural Model

The structural model of the aircraft, shown in Figure 1, is a beam-stick finite element model built in the commercial solver Nastran. The fuselage, wing, engine pylons and tailplanes are represented by bar elements (CBAR) and rigid elements (RBE2) are used to connect the different subcomponents. The mass distribution is represented both by distributed masses on the bar elements, for the structural mass, and by lumped masses (CONM2), these accounting for the engines, systems, furniture, payload and fuel.

The structural dynamics equations are formulated via the modal approach and selecting the first 30 normal modes of the free-free structure, including the 6 rigid body modes, to obtain the modal mass, damping and stiffness matrices, namely M_{hh}, C_{hh} and K_{hh}. This subset of lower frequencies modes is sufficient to obtain converged airframe loads.

Aerodynamic Model

The aerodynamic model is based on the Doublet Lattice Method (DLM) available in Nastran. The DLM is a 3D subsonic unsteady panel code formulated in the frequency domain and has long established itself as the standard methodology employed in the industry for aeroelastic calculations. The wing and tailplanes are modelled by a flat plate mesh, whereas the aerodynamic effect of the fuselage is neglected. The model contains also control surfaces

(elevator, rudder and ailerons). The interpolation between the structural and aerodynamic meshes is based upon the Infinite Plane Spline method [7]. The DLM provides the Generalized Aerodynamic Forces (GAF) due to structural motion, gust disturbance and control surfaces deflections as complex matrices tabulated as a function of Mach number and a finite set of n_k reduced frequencies, namely $Q_{hh}(M, k)$, $Q_{hg}(M, k)$ and $Q_{hc}(M, k)$.

Flight Control System

The control surfaces of the aircraft are driven by servo-hydraulic actuators. The modelling of the actuator follows [8]. Its dynamics is represented as a 3rd order transfer function between the pilot input u_c and the actual control surface deflection δ. The open-loop transfer function of the actuator relates the control surface deflection to the displacement of the servo-valve spool u_v

$$G(s) = \frac{\delta}{u_v} = \frac{g}{s\left(\frac{s^2}{\omega_h^2} + \frac{2\zeta}{\omega_h}s + 1\right)}$$

(1)

where ω_h is the hydraulic angular frequency, ζ the hydraulic damping and g the gain. Since the equations governing the actuator dynamics are non-linear, to obtain the transfer function these are linearized in the neighborhood of an operating point, assumed to be the neutral position of the valve spool. A feedback between the valve spool displacement and the desired input u_c is introduced and the closed-loop transfer function becomes

$$H_c(s) = \frac{\delta}{u_c} = \frac{k_c G(s)}{1 + k_c G(s)}$$

(2)

with k_c being the proportional gain.

Under this modelling assumption, the actuator acts as a shaping filter of the pilot input command and in series with the aeroelastic plant.

State-Space Model

The classical approach used in aeroelasticity for loads and flutter analyses solves the equations of motion in the frequency domain. To apply the Model Order Reduction method presented in this paper, the equations of motion must be translated into the time domain and casted in state-space form, leading to the Linear Time Invariant system

$$\dot{x}_{ae} = A_{ae}x_{ae} + B_{ae}u$$
$$y = C_{ae}x_{ae} + D_{ae}u$$

(3)

where $\dot{x}_{ae}$ are the states of the aeroservoelastic system, including the structural, aerodynamic and actuator states, u is the input exciting the aircraft, a gust or a pilot command, and y the output, loads on the airframe or other Interesting Quantities (IQ).

Since the aerodynamic forces are available in the frequency domain in tabulated form, to obtain Eq. (3) a Rational Function Approximation (RFA) of the matrices $\boldsymbol{Q_{hh}}(M,k)$ and $\boldsymbol{Q_{hg}}(M,k)$ is performed. This consists of approximating the aforementioned matrices by a rational polynomial in the Laplace variable s such that

$$\widetilde{\boldsymbol{Q_{hh}}}(s,M) = \boldsymbol{D_0} + \frac{l_a}{V}\boldsymbol{D_1}s + \left(\frac{l_a}{V}\right)^2 \boldsymbol{D_2}s^2 + \boldsymbol{C_a}\left(s\boldsymbol{I} - \frac{V}{l_a}\boldsymbol{A_a}\right)\boldsymbol{B_a}s$$

$$\widetilde{\boldsymbol{Q_{hg}}}(s,M) = \boldsymbol{D_{0g}} + \frac{l_a}{V}\boldsymbol{D_{1g}}s + \left(\frac{l_a}{V}\right)^2 \boldsymbol{D_{2g}}s^2 + \boldsymbol{C_g}\left(s\boldsymbol{I} - \frac{V}{l_a}\boldsymbol{A_g}\right)\boldsymbol{B_g}s$$

(4)

Many approaches have been developed to perform this approximation; in the following Roger's method [9] is employed. It assumes that Eq. (4) are rewritten as

$$\widetilde{\boldsymbol{Q_{hh}}}(s,M) = \boldsymbol{D_0} + \frac{l_a}{V}\boldsymbol{D_1}s + \left(\frac{l_a}{V}\right)^2 \boldsymbol{D_2}s^2 + \frac{V}{l_a}\sum_{l=1}^{n_a}\frac{s}{s+\frac{V}{l_a}\beta_l}\boldsymbol{A_l}$$

$$\widetilde{\boldsymbol{Q_{hg}}}(s,M) = \boldsymbol{D_{0g}} + \frac{l_a}{V}\boldsymbol{D_{1g}}s + \frac{V}{l_a}\sum_{l=1}^{n_g}\frac{s}{s+\frac{V}{l_a}\beta g_l}\boldsymbol{A_{gl}}$$

(5)

In the original formulation the unknowns are the coefficients of $\boldsymbol{D_0}$, $\boldsymbol{D_1}$, $\boldsymbol{D_2}$ and $\boldsymbol{A_l}$, while the number and values of the aerodynamic poles β_l are selected a-priori and $\beta_l < 0$ to ensure asymptotic stability. The coefficients of the polynomial are then identified by a linear least-square procedure applied term by term to the matrix $\boldsymbol{Q_{hh}}$, i.e. a curve fitting is performed. In this work, Roger's formulation is extended considering the aerodynamic poles as free design variables of an optimization process whose objective function is the minimization of the squared error between the approximated and tabulated GAF. Several studies have been published on the nonlinear optimization of the aerodynamic poles [10,11,12]. In the present work, nonlinear non-gradient constrained optimizations are performed to select the aerodynamic poles minimizing the following objective function

$$\mathcal{F} = \sum_{j=1}^{n_h}\left(\sum_{i=1}^{n_h}\sum_{m=1}^{n_k}w_{ij}\varepsilon_{ijm}\right)^{1/2}$$

$$\varepsilon_{ij} = \frac{|\widetilde{Q_{ij}} - Q_{ij}|^2}{max_m\{1, |Q_{ij}|^2\}}$$

(6)

Where w_{ij} are weighting factors that can be chosen if some specific elements of the GAF matrices are deemed more important to be approximated accurately. The whole RFA procedure consists thus of a two-level optimization: an inner linear least-square curve fitting for the coefficients matrices at the numerator of Eq. (5) and an outer nonlinear optimization for the aerodynamic poles β_l.

The GAF of the control surfaces are instead cast into time domain through a quasi-steady approximation so that

$$\widetilde{\boldsymbol{Q_{hc}}}(s,M) = \boldsymbol{D_{0c}} + \frac{l_a}{V}\boldsymbol{D_{1c}}s + \left(\frac{l_a}{V}\right)^2 \boldsymbol{D_{2c}}s^2 =$$

$$= \boldsymbol{Q_{hc}}(0,M) + \frac{l_a}{V}\boldsymbol{Q'_{hc}}(0,M)s + \frac{1}{2}\left(\frac{l_a}{V}\right)^2 \boldsymbol{Q''_{hc}}(0,M)s^2$$

(7)

Optimized Rational Function Approximation

The RFA is performed employing and comparing three non-gradient optimization algorithms: a Nelder-Mead simplex scheme, both in its unconstrained and constrained bounded version [13], a genetic algorithm [14] and simulated annealing [15]. As indicators of the goodness of the fit, the total root mean square error and the Frequency Response Assurance Criterion (FRAC) are calculated as

$$ERR = \frac{1}{\sqrt{n_k}}\sum_{j=1}^{n_h}\left(\sum_{i=1}^{n_h}\sum_{m=1}^{n_k}w_{ij}\varepsilon_{ijm}\right)^{1/2}$$

$$FRAC_{ij} = \frac{|\widetilde{\boldsymbol{Q_i}}(ik)^T\boldsymbol{Q_j}(ik)|^2}{|\widetilde{\boldsymbol{Q_i}}(ik)^T\widetilde{\boldsymbol{Q_i}}(ik)|\cdot|\boldsymbol{Q_j}(ik)^T\boldsymbol{Q_j}(ik)|}$$

(8)

The RFA of $\boldsymbol{Q_{hh}}$ is performed assuming 5 aerodynamic poles at 14 reduced frequencies. The total root mean square error for the unoptimized and the three optimization algorithms is reported in Table 2. For the same number of aerodynamic poles, there is an improvement of the curve fitting error for the optimized RFAs. It is interesting to note that the three algorithms deliver different poles, but the total error is comparable.

Table 2. Total root mean square error for unoptimized and optimized Q_{hh} RFAs

Method	ERR	Aerodynamic poles
RFA standard	1.290E-03	0.057, 0.227, 0.510, 0.907, 1.417
RFA Nelder-Mead	6.422E-04	0.520, 0.689, 0.741, 0.999, 1.001
RFA Genetic Algorithm	5.309E-04	0.633, 0.784, 0.869, 1.041, 1.106
RFA Simulated Annealing	5.135E-04	0.698, 0.899, 0.932, 0.973, 1.189

The optimized RFA shows most of its benefit particularly for the approximation of the gust aerodynamic force matrix $\boldsymbol{Q_{hg}}$. It is known that the terms of this matrix show a spiral behavior at high reduced frequencies in the Re-Im plane, due to the penetration term, that are difficult to approximate with rational polynomials [16]. The optimization of the poles introduces additional design variables which can be tuned to improve the curve fitting.

The curve fit of four elements of $\boldsymbol{Q_{hg}}$, computed with the same four approaches and assuming 6 aerodynamic poles, is presented in Figure 2 and the FRAC for the standard and Genetic Algorithm RFA in Figure 3; the total root mean square error and the resulting aerodynamic poles are given in Table 3. The improvement is confirmed, especially at high reduced frequencies where the spiral behavior is significant.
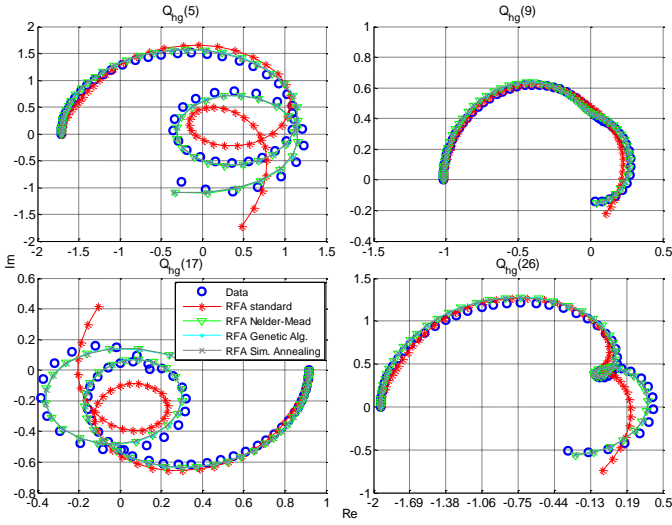
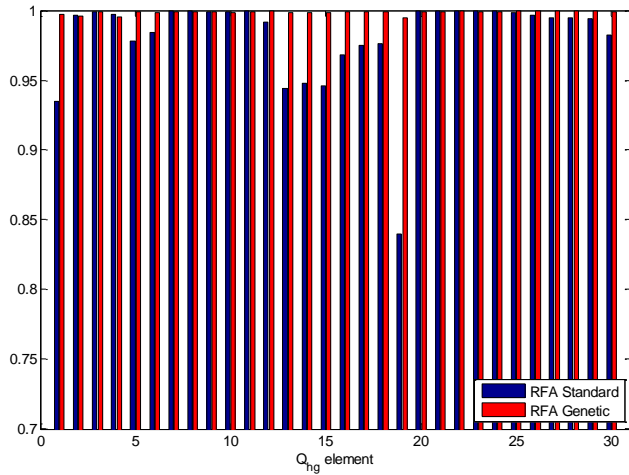Figure 2. Curve fit for different RFA methods of four Q_{hg} elements

Figure 3. FRAC comparison between standard (unoptimized) RFA and RFA optimized using Genetic Algorithm of Q_{hg}

Table 3. Total root mean square error for unoptimized and optimized gust RFAs

Method	ERR	Aerodynamic poles
RFA standard	6.716E-01	0.032, 0.128, 0.289, 0.513, 0.802, 1.154
RFA Nelder-Mead	2.211E-01	0.662, 0.663, 0.668, 0.670, 0.689, 0.693
RFA Genetic Algorithm	2.228E-01	0.652, 0.658, 0.668, 0.682, 0.683, 0.708
RFA Simulated Annealing	2.257E-01	0.570, 0.616, 0.626, 0.752, 0.769, 0.770

Once the RFAs of Q_{hh} and Q_{hg} are performed, the aeroelastic equations of motion can be cast into state-space form Eq. (3), where the state-space matrices are

$$A_{ae} =$$
$$= \begin{bmatrix} 0 & I & 0 & 0 \\ -M_{ae}^{-1}(K_{hh} - q_\infty D_0) & -M_{ae}^{-1}(C_{hh} - q_\infty \frac{l_a}{V} D_1) & q_\infty M_{ae}^{-1} C_a & M_{ae}^{-1} C_g \\ 0 & B_a & \frac{V}{l_a} A_a & 0 \\ 0 & 0 & 0 & \frac{V}{l_a} A_g \end{bmatrix}$$

$$B_{ae} = q_\infty \begin{bmatrix} 0 & 0 \\ M_{ae}^{-1} D_{0g} & M_{ae}^{-1} \frac{l_a}{V} D_{1g} \\ 0 & 0 \\ 0 & B_g \end{bmatrix}$$

$$C_{ae} = [IL \quad 0 \quad 0 \quad 0]$$

$$D_{ae} = 0$$

(9)

with

$$M_{ae} = M_{hh} - q_\infty \left(\frac{l_a}{V}\right)^2 D_2$$

(10)

And IL is the matrix whose columns contain the airframe loads (bending moment, shear, torque) due to each normal mode retained in the analysis.

The control surfaces deflections δ are linked to the pilot command via the transfer function Eq. (2). This is transformed from the Laplace domain to a state-space form through a controllable canonical realization [17] in series with the aeroelastic state-space model.

The final states vector of the aeroservoelastic system contains the modal displacement and velocities, the aerodynamic states arising from the RFA of Q_{hh} and Q_{hg} and the actuator states

$$x_{ase} = [q_h, \dot{q}_h, x_a, x_g, x_{actu}]^T$$

(11)

The input vector u contains the gust velocity and its time derivative w_g and $\dot{w}_g$ and the desired elevator deflection δ and its first and second time derivatives. Gust responses and flight maneuvers are therefore simulated by integration of the state-space equations through the state transition matrix [17].

To further confirm the validity of the RFA and to ensure that the aircraft considered does not show unstable response, a flutter analysis is performed by the standard Nastran PK method (frequency-domain) and by the RFA. The comparison of the flutter diagrams obtained by the two methods is presented in Figure 4. The results show a good agreement between the frequency-domain and time-domain analysis, both for the damping and frequency predictions. Two modes show flutter at a very high speed, well above $1.2V_D$. The major differences are in the damping of the highly damped modes, but these are less relevant than the flutter speed and frequency, which are predicted with an error less than -0.4%.
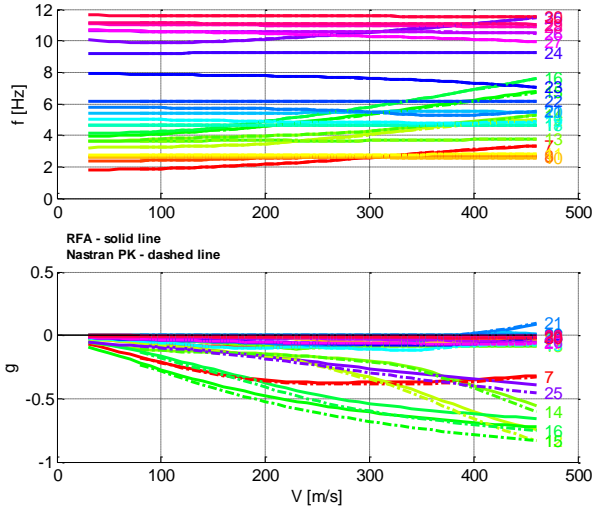
Figure 4. Flutter diagram comparison between Nastran PK and RFA, unmatched analysis at Mach 0.60

Model Order Reduction

Model Order Reduction (MOR) is a mathematical technique applied to reduce the size of a numerical model. The original Full Order Model (FOM) is approximated by a low-dimensional Reduced Order Model (ROM) which can retain a good accuracy with a significant speed-up of the simulation time. This saving in computational time is particularly beneficial for an aircraft loads calculation process, where thousands of analyses are required to show compliance with the certification requirements. The total number of states of the aeroservoelastic system Eq. (11) is given by

$$N = 2n_h + n_h(n_a + n_g) + 3n_{actu}$$

(12)

where n_h is the number of structural modes retained, n_a and n_g the number of aerodynamic poles for the RFA of the GAF due to the structural motion and gust and n_{actu} the number of control surface actuators. For the present model it equals 393. Although this figure is not as high as in other engineering applications, there is still a benefit in reducing the model's size since the number of flight conditions, gust lengths, maneuvers and mass configurations that have to be considered to evaluate flight loads could easily lead to hundreds of thousands of simulations.

An extensive overview of MOR is given by Antoulas in [6]. All the existing methods are projection-based, that is they seek to find an approximation of the FOM states into a lower dimensional subspace. Considering a LTI system such as the one of Eq. (3), a ROM of order $n_r \ll N$ is determined by applying left and right projectors $W \in \mathbb{R}^{N \times n_r}$ and $V \in \mathbb{R}^{N \times n_r}$ to the FOM matrices

$$A_r = (W^T V)^{-1} W^T A V$$

$$B_r = (W^T V)^{-1} W^T B$$

$$C_r = CV$$

(13)

The right and left projection matrices $W \in \mathbb{R}^{N \times n_r}$ and $V \in \mathbb{R}^{N \times n_r}$ are referred as the Reduced Order Basis (ROB) and the methods used to calculate these fall into three categories [6]:

- Krylov subspace methods
- Balanced Truncation
- Proper Orthogonal Decomposition

Balanced Truncation is chosen as the reduction technique. It is commonly employed in the control system field and has desirable properties such as stability preservation and an H_∞ error bound. For more details refer to [6].

Balanced Truncation transforms the original states to a subspace where the new states each corresponds to a Hankel singular value σ_k, which is a measure of the importance of that state in the input-to-output relation. The states associated with the smallest Hankel singular values can be discarded and the H_∞ error bound of the resulting ROM is guaranteed to satisfy

$$err_{H_\infty} \le 2 \sum_{k=n_r+1}^{N} \sigma_k$$

(14)

The right and left bases computed by BT are one the inverse of the other, i.e. $W^T = T_B$, $V = T_B^{-1}$ and $W^T V = I$, therefore Eq. (13) become

$$A_r = T_B A T_B^{-1}$$

$$B_r = T_B B$$

$$C_r = C T_B^{-1}$$

(15)

Results

The procedure presented is applied to the gust response and pitching maneuver simulation of the generic transport aircraft. The IQs monitored are the integrated loads (bending moment, shear and torque) along the wing and horizontal tail and the vertical load factor.

Gust response

CS-25 and FAR-25 specify the discrete gust load cases required for certification (CS 25.341 and FAR 25.341) considering the aircraft in level flight and subject to symmetrical vertical and lateral gust with a "1-cosine" velocity profile having a gust gradient H (half of the gust wavelength) and a maximum gust velocity w_{g0} (Eq. (16)). Different gust gradients between 30ft and 350ft must be investigated to determine the critical condition for each load quantity.

$$w_{g0} = w_{ref} \left(\frac{H}{350}\right)^{1/6}$$

$$w_g(s) = \frac{w_{g0}}{2} \left[1 - \cos \frac{\pi s}{H}\right]$$

(16)

For the present analysis, the state-space FOM and ROM are assembled in a specific flight condition, altitude 25000ft and Mach number 0.60.

Balanced Truncation is applied to reduce the model size from 393 states to 24 states. Two FRFs of the original and reduced order systems (gust to wing root bending moment and gust to wing root torque) are compared in Figure 5 and a good matching can be clearly seen in the frequency range of interest. The Hankel singular values of the balanced system are also presented in Figure 6 to show their rapid decay, which allow retaining a limited number of states without loss of accuracy.
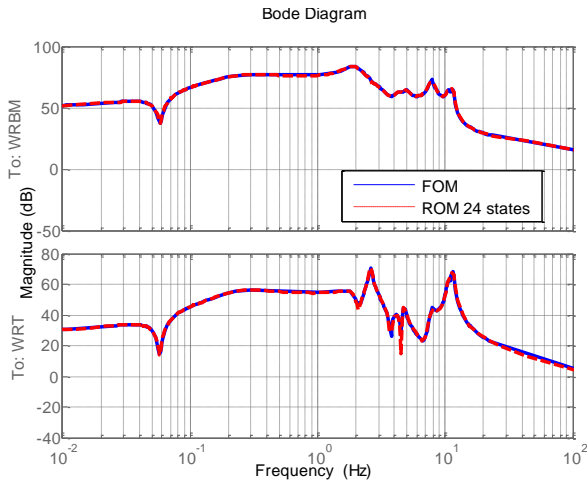
Figure 5. FRFs of the FOM and ROM
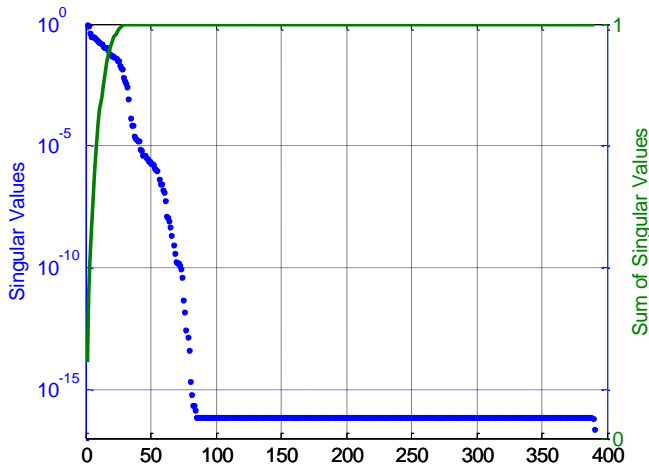
Figure 6. Hankel singular values of the system after balanced truncation

Subsequently, gust responses with ten different gust gradients are simulated. The FOM and ROM bending moment at the wing root and the torque at the wing engine inboard sections are presented in Figure 7 and Figure 8 for all the gust gradients. The loads shown are the incremental ones, i.e. those generated only by the gust to which the 1g level flight loads must be superimposed.

Two dimensional load envelopes of the considered gust family are obtained, on each load monitoring sections, by plotting the time history one IQ vs. another, for instance bending moment vs. torque, and taking the convex hull of this set of points. The resulting 2D plots

(sometimes called "potato plots") represent correlated loads, that is loads acting at the same time instant on the airframe and balanced, and are among the most common critical load selection criteria employed. Figure 9 and Figure 10 present such plots for the wing root and wing engine inboard sections, comparing the FOM and the ROM. The colored dashed lines represent the torque vs. bending moment plots for each gust gradients, whose envelope is the correlated loads plot.

As shown by these results, the agreement between the FOM and the ROM is excellent, both in terms of time histories and of load envelopes. The number of states selected for the ROM is mainly dictated by having a good prediction of the torque, associated with higher frequencies modes, whereas the bending moment is accurately computed even with a smaller ROM.

The speed-up obtained with the ROM is significant: for the gust responses considered the saving in computational time reaches 78%. Whereas for the FOM most of the computational time is taken by the integration itself (94% of the total time), for the ROM the expensive phase is the generation of the balanced truncation, accounting for 65% of the total computational time.
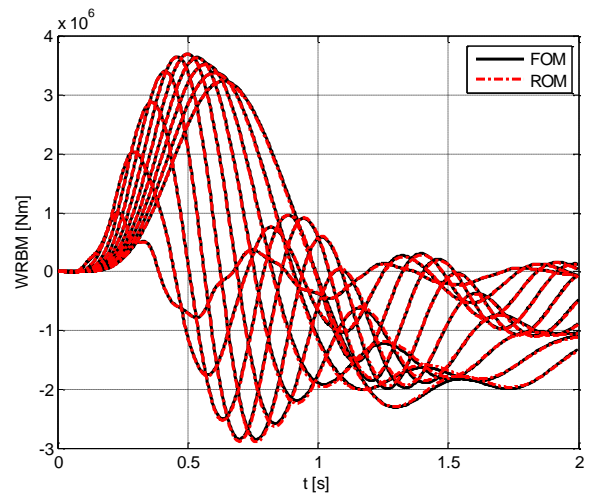

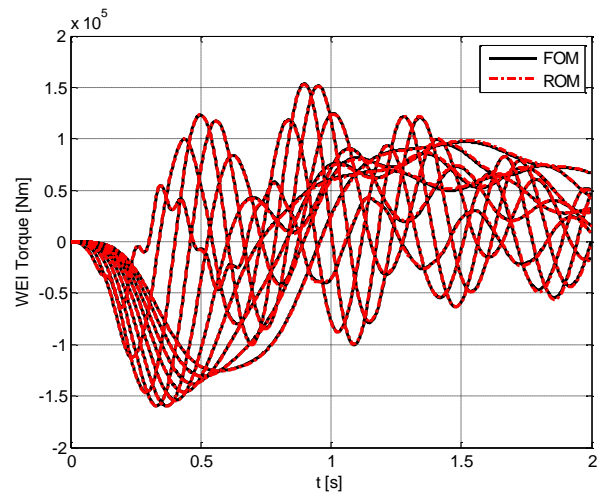Figure 7. Wing root bending moment for 10 gust gradients, FOM vs. ROM

Figure 8. Wing engine inboard torque for 10 gust gradients, FOM vs. ROM
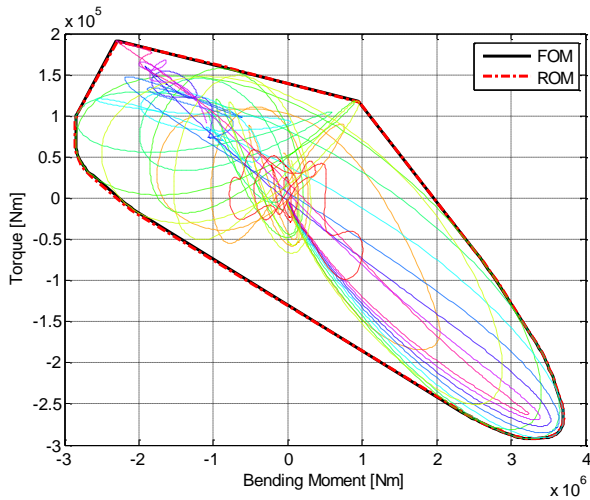
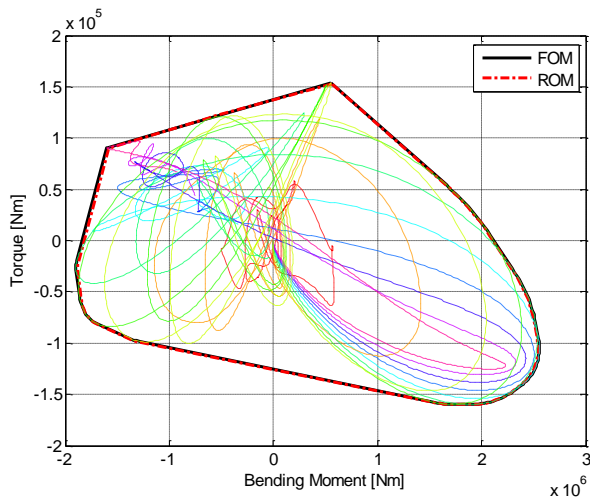Figure 9. Correlated loads plot at the wing root for a gust family, FOM vs. ROM

Figure 10. Correlated loads plot at the wing engine inboard section for a gust family, FOM vs. ROM

Comparison with Pratt's formula

In the past decades gust loads have been determined for long with quasi-static methods [18], which greatly simplify the complexity, and associated time, of the calculations involved. Over the years various formulas have been proposed [18], in particular Pratt's formula [19] has been successfully adopted by the industry and still today, for Part 23 aircraft, it is the standard approach required. Part 25, on the other hand, mandates for more rational analysis taking into account load redistribution due to deformation and unsteady aerodynamics.

The gust load factors and wing loads obtained applying Pratt's formula and performing a dynamic analysis in time-domain are now presented.

Pratt's formula calculates the incremental load factor at the aircraft CG due to a gust as:

$$\Delta n_z = K_g \frac{\rho w_{g0} V C_{L\alpha}}{2W/S}$$

(17)

where W/S is the wing loading, ρ the air density, V the airspeed, $C_{L\alpha}$ the aircraft lift curve slope and K_g the so-called gust alleviation factor.

Assuming the flight condition previously specified (M 0.60, 25000ft), which corresponds to $K_g = 0.7975$, the gust load factors computed by Eq. (17) and by dynamic simulation ("1-cosine" velocity profile) are compared in Figure 11 for ten gust gradients. There is a good matching between the two methodologies for gust gradients between 10 and 12 chords, which is to be expected since Pratt's formula has been derived assuming a gust gradient of 12.5 chords. As the gust gradient decreases the mismatching increases because smaller gust gradients have higher frequency content (see Eq. (16)) that excites more the flexible modes, whereas longer gust gradients excite predominantly rigid body modes.

Once the gust load factor has been computed by Pratt's formula, to obtain the loads along the wingspan a rigid trim analysis at this specific load factor is performed. The resulting bending moment along the wingspan is shown in Figure 12 alongside with the bending moment calculated by dynamic response at the gust gradient and time instant of maximum wing root bending moment (10.5 chords). The latter is higher than the former along the whole wingspan, with dynamic amplification factors between 1.13 and 1.18.

It is clear that a quasi-static analysis could lead to a non conservative estimation of the loads whenever the effects of the structural dynamics and unsteady aerodynamics are relevant, such as for modern transport aircraft where the lowest wing elastic frequencies are in the order of few Hz.
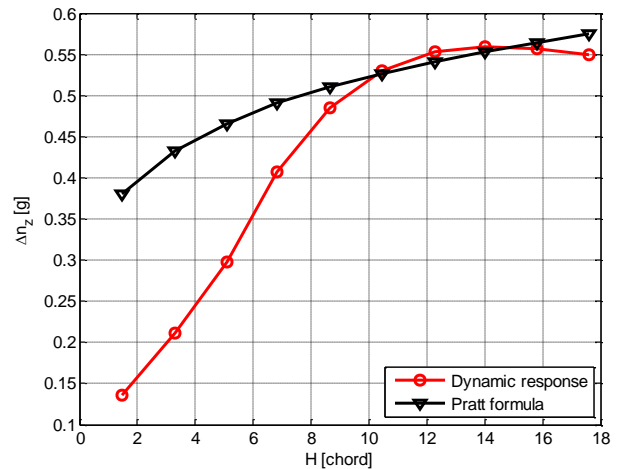

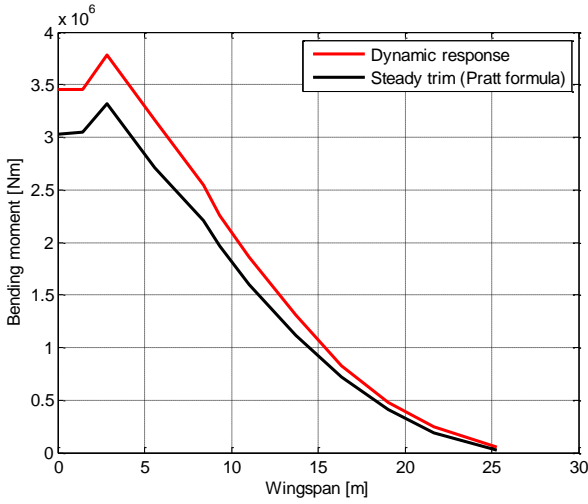Figure 11. Gust load factor vs. gust gradient by Pratt's formula and dynamic response

Figure 12. Wing bending moment for critical gust gradient by steady trim at Pratt's formula load factor and dynamic response

Pitching maneuver

Certification requirements cover two types of symmetric maneuvers: unchecked and checked. The abrupt unchecked pitching involves, with the aircraft in steady flight up to V_A, a sudden displacement of the pitch control (elevator) so as to yield the maximum positive load factor; the response needs not to be considered after this limit, or the maximum tail load, has been reached. The checked pitching maneuver, starting with the aircraft in steady flight between V_A and V_D, considers both nose-up and nose-down pitching obtained applying a displacement of the pitch control defined as

$$\delta(t) = \delta_1 \sin(\omega t) \qquad 0 < t \leq t_1, \qquad t_1 = \pi/2\omega$$

$$\delta(t) = \delta_1 \qquad t_1 < t \leq t_2, \qquad t_2 = t_1 + \Delta t$$

$$\delta(t) = \delta_1 \sin(\omega[t + t_1 - t_2]) \qquad t_2 < t \leq t_{max}, \ t_{max} = t_2 + \pi/\omega$$

$$(18)$$

where the circular frequency ω is taken equal to the undamped natural frequency of the short period mode of the aircraft, but not less than $\omega = \pi V/2V_A$. The maximum deflection applied δ_1 and the holding time Δt must be selected to achieve, and not exceed, the positive limit load factor, for initial nose-up maneuvers, or a load factor of $0g$, for initial nose-down maneuvers.

For the checked pitching both the elevator deflection δ_1 and the holding time Δt can be tuned to reach the required load factor, resulting in an underdetermined problem. The actual elevator time history is then found through an optimization, where the objective function is the sum of two terms properly weighted, one chosen to achieve the target load factor and the other to maximize a specific IQ, for instance the squared sum of the horizontal tail bending moment and torque. The elevator deflection has upper and lower bounds set to the maximum available deflection and the holding time must not exceed $5s$. This optimization is considerably faster when performed via the ROM than with the FOM.

Pitching maneuvers simulations are carried out at Mach 0.60 and 25000ft with the same FOM and ROM previously presented. The

vertical load factor at the CG (incremental) for a nose-up and nose-down abrupt pitching maneuver is shown in Figure 13. The simulation is stopped once the aircraft reaches the maximum or minimum load factor. Figure 14 presents the correlated load plot for a checked pitching maneuver at the horizontal tail root section, which is usually sized by this type of load case. These results confirm that also for flight maneuvers the ROM is capable of delivering accurate results with a significant saving in computational time, which, for these simulations, reaches 60%.
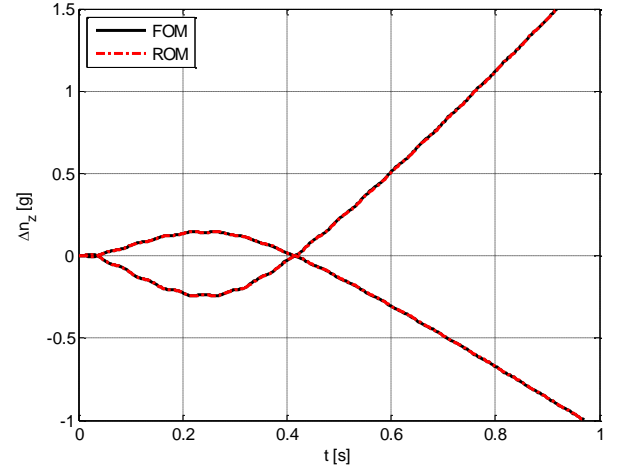

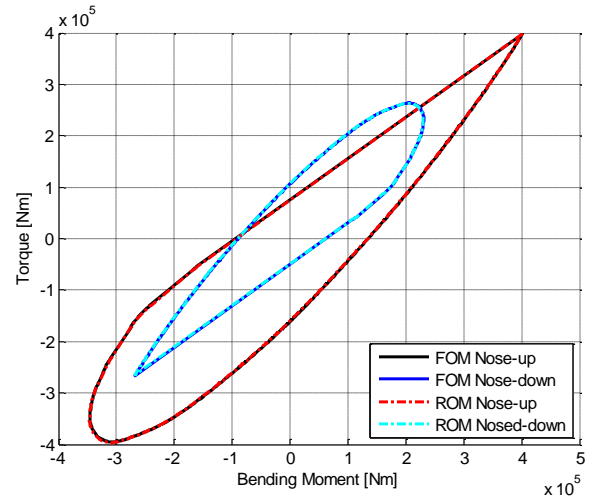Figure 13. Aircraft load factor during a nose-up and nose-down unchecked pitching maneuver, FOM vs. ROM

Figure 14. Correlated loads plot at the horizontal tail root for a nose-up and nose-down checked pitching maneuver, FOM vs. ROM

Conclusions

A technique to generate a Reduced Order Model in time domain of a generic transport aircraft has been presented. It includes the main elements of aeroservoelastic models commonly employed in an industrial environment, i.e. airframe flexibility, unsteady aerodynamics and actuator dynamics. The reduced size model is used to run gust responses and pitching maneuver simulations to compute airframe loads. It is demonstrated that the accuracy of the ROM is excellent whereas the computational time is significantly reduced. A

further development of the method pursues the fast and efficient generation of the ROM at different flight conditions, to cover all the points in the flight envelope that must be analyzed in the loads process, by interpolating a database of ROMs built at a few selected points of the flight envelope. Such procedure is built upon the framework proposed in this paper and it is presented by Castellani et al. in [20].

References

1. EASA, Certification Specification for Large Aeroplanes CS-25 Amendment 3, September 2007.
2. FAA, Part 25 Airworthiness Standard Transport Category.
3. Wright, J. R., and Cooper, J. E., "Introduction to Aircraft Aeroelasticity and Loads," Wiley, 2007, ISBN 978-0470858400.
4. Bisplinghoff, R. L., Ashley, H., and Halfman, R. L., "Aeroelasticity," Dover, 1996, ISBN 978-0486691893.
5. Tiffany, S. H., and Karpel, M., "Aeroservoelastic Modeling and Applications using Minimum-State Approximations of the Unsteady Aerodynamics," NASA TM-101574, 1989.
6. Antoulas, A. C., "An Overview of Approximation Methods for Large-Scale Dynamical Systems," *Annual Reviews in Control*, 29(2):181-190, 2005, doi:10.1016/2005-08-0002.
7. Harder, R. L., and Desmarais, R.N., "Interpolation using Surface Splines," *AIAA Journal*, 9(2):189-191, 1972, doi:10.2514/3-4430.
8. Belardo, M., Pecora, M., and Paletta, N., "Flutter Analysis with Hydraulic Servos-a Technique for Modeling Actuator Dynamics," SAE Technical Paper 2013-01-2194, 2013, doi:10.4271/2013-01-2194.
9. Roger, K. L., "Airplane Math Modeling Methods for Active Control Design," AGARD CP-228, 1977.
10. Tiffany, S. H., and Adams, W. M., Jr., "Nonlinear Programming Extensions to Rational Function Approximation for Unsteady Aerodynamic Forces," NASA TP-2776, 1988.
11. Eversman, W., and Tewari, A., "Consistent Rational-Function Approximation for Unsteady Aerodynamics," *Journal of Aircraft*, 28(9):545-552, 1991, doi:10.2514/3-46062.
12. Karpel, M., and Strul, E, "Minimum-State Unsteady Aerodynamic Approximations with Flexible Constraints," *Journal of Aircraft*, 33(6):1190-1196, 1996, doi:10.2514/3-47074.
13. Luersen, M. A., Le Riche, R., and Guyon, F., "A constrained, globalized, and bounded Nelder–Mead method for engineering optimization," *Structural and Multidisciplinary Optimization*, 27(1-2):43-54, 2004, doi:10.1007/00158-003-0320-9.
14. Goldberg, D. E., "Genetic Algorithms in Search, Optimization and Machine Learning," Addison-Wesley, 1989, ISBN 978-0201157673.
15. Kirkpatrick, S., Gelatt, C. D., and Vecchi, M. P., "Optimization by Simulated Annealing," *Science*, 220(4598):671-680, 1983, doi:10.1126/220-4598-671.
16. Karpel, M., Moulin, B., and Chen, P. C., "Dynamic Response of Aeroservoelastic Systems to Gust Excitation," *Journal of Aircraft*, 42(5):1264-1272, 2005, doi:10.2514/1-6678.
17. Friedland, B., "Control System Design: An Introduction to State-Space Methods," Dover, 2005, ISBN 978-0486442785.
18. Ricciardi, A., P., Patil, M., J., Canfield, R., A., and Lindsley, N., "Utility of Quasi-Static Gust Loads Certification Methods for Novel Configurations," presented at 52nd AIAA/ASME/ASCE/AHS/ASC Structures, Structural Dynamics and Materials Conference, USA, 4-7 April 2011.
19. Pratt, M., and Walker, W., "A Revised Gust-Load Formula and a Reevaluation of V-G Data Taken on Civil Transport Airplanes from 1933 to 1950," NACA TR-1206, 1954.
20. Castellani, M., Lemmens, Y., and Cooper, J. E., "Parametric Reduced Order Model for Rapid Prediction of Dynamic Loads and Aeroelastic Response with Structural Nonlinearities," presented at International Forum on Aeroelasticity and Structural Dynamics, St. Petersburg, Russia, 28 June-02 July 2015.

Acknowledgments

Definitions/Abbreviations

ROM	Reduced Order Model
MOR	Model Order Reduction
LTI	Liner Time Invariant
DLM	Doublet Lattice Method
GAF	Generalized Aerodynamic Forces
RFA	Rational Function Approximation
FRF	Frequency Response Function
CG	Center of Gravity